Identification of novel toxin domains and characterization of a broadly distributed family of lipid-targeting NlpC/P60

Gianlucca G. Nicastro[b, c, ¥], Stephanie Sibinelli-Sousa[b, ¥], Julia Takuno Hespanhol[a], Thomas W. C. Santos[b], Joseph P. Munoz[a], Rosangela S. Santos[d], Blanca M. Perez-Sepulveda[e], Sayuri Miyamoto[d], L. Aravind[c], Robson F. de Souza[b,#], Ethel Bayer-Santos[a,b,f#].

[a]Department of Molecular Biosciences, College of Natural Sciences, The University of Texas at Austin, Austin, USA.

[b]Departamento de Microbiologia, Instituto de Ciências Biomédicas, Universidade de São Paulo, São Paulo, Brazil.

[c]Computational Biology Branch, National Center for Biotechnology Information, National Library of Medicine, National Institutes of Health, USA.

[d]Departamento de Bioquímica, Instituto de Química, Universidade de São Paulo, São Paulo, Brazil.

[e]Institute of Infection, Veterinary and Ecological Sciences, University of Liverpool, Liverpool, UK.

[f]LaMontagne Center for Infectious Disease, The University of Texas at Austin, Austin, Texas, USA.

Running title: Novel toxin domains and lipid-targeting NlpC/P60

#Corresponding authors: ebayersantos@austin.utexas.edu; rfsouza@usp.br

[¥]These authors contributed equally to this work. Author order was determined on the basis of seniority.

Abstract: Bacterial warfare is a common and ancient phenomenon in nature, where bacterial species use strategies to inhibit the growth or kill competitors. This involves the production and deployment of antibacterial toxins that disrupt essential cellular processes in target cells. Polymorphic toxins comprise a group of offensive systems with a modular structure featuring a conserved N-terminal translocation domain fused to diverse C-terminal toxin domains. The continuous arms race in which bacteria acquire new toxin and immunity proteins to promote increased adaptation to their environment is responsible for the diversification of this toxin repertoire. Here, we deployed *in-silico* strategies to analyze 10,000 genomes and identify toxin domains secreted via the type VI secretion system of *Salmonella*. We identified and manually curated 128 candidates, which are widespread polymorphic toxins detected in a vast array of species and linked to diverse secretion systems. In addition, 45 previously uncharacterized toxin domains were identified. STox15 was among the most frequent candidates found in the dataset and was selected for in-depth characterization. STox15 is an antibacterial effector belonging to the NlpC/P60 papain-like fold superfamily with a permuted catalytic core typical of lipid-targeting versions rather than peptidases or amidases. Biochemical analysis with recombinant protein and lipidomics of intoxicated *Escherichia coli* revealed that STox15 displays phospholipase activity cleaving off acyl groups from phosphatidylglycerol and phosphatidylethanolamine. **Importance:** This work broadens our understanding of polymorphic toxin domains and provides the first direct characterization of a lipid-targeting NlpC/P60 domain in biological conflicts.

Keywords: Polymorphic toxins, bacterial toxins, NlpC/P60, phospholipase, acyltransferase.

Introduction

Competition is a fundamental biological process in nature, occurring both within and between species that share a common environment. Bacteria actively participate in these ecological battles employing a potent arsenal of toxins as their weaponry[1]. A prominent mechanism for toxin delivery among Gram-negative bacteria is via the type 6 secretion system (T6SS)[2]. Phylogenetic analysis of T6SS components showed that there are four types of T6SSs (T6SS$^{i\text{-}iv}$)[3-5], with the canonical T6SS^{i} present in *Proteobacteria* being further classified into six subtypes (i1, i2, i3, i4a, i4b and i5)[4,6,7]. The T6SS functions in a contact-dependent manner and rely on the biochemical properties of secreted effector toxins for its function[8]. These toxins frequently recombine and move via lateral gene transfer, allowing them to be delivered by different secretion systems, which warrants their name as polymorphic toxins[9]. During secretion via the T6SS, toxins are loaded onto a spear-like structure formed by hexameric rings of Hcp proteins capped by a spike comprising a trimer of VgrG sharpened by a PAAR protein[10]. Effectors are translocated into target cells either fused at the C-terminus of Hcp, VgrG, and PAAR proteins (named specialized effectors), or associated with these proteins via adaptors (cargo effectors)[11]. Antibacterial toxins are often paired with immunity proteins that prevent self-intoxication, thus forming gene pairs that are frequently located near structural components of the T6SS[8,12].

The protective role of the endogenous microbiota against *Salmonella* infection has been recognized for years[13]; however, only recently have studies started to reveal the mechanism by which the microbiota maintains gut homeostasis and promotes colonization resistance[14]. Despite this understanding, there is a relative scarcity of information about the direct antimicrobial mechanisms employed by commensals and pathogens during these disputes for niche control[15]. T6SSs clusters are conserved across

several *Salmonella* spp., highlighting their importance to the fitness of these bacteria[16,17]. *Salmonella* spp. encode T6SSs in different pathogenicity islands (SPIs), which were acquired by distinct horizontal transfer events[16,17]. *S.* Typhimurium encodes a T6SS subtype i3 within SPI-6, which is important for interbacterial competition and gut colonization in mice[18,19]. There is limited information about the identity or mechanism of the T6SS effector repertoire that contributes to these phenotypes.

Here, we set out to identify the repertoire of T6SS effectors in a dataset of 10,000 *Salmonella* isolates utilizing a computational approach, followed by careful manual curation. Employing sensitive sequence and structure searches alongside comparative genomics, we identified 128 candidates, including 45 new toxin domains which were not recognized in publicly available databases, and are widespread among several species. This comprehensive analysis indicates that *Salmonella* T6SSs subtypes i3 and i1 are associated with antibacterial and anti-eukaryotic effectors, respectively. Furthermore, our findings reveal that each of the 149 serovars contained in the dataset harbors a unique combination of effectors, likely required for their specific ecological interactions. A detailed examination of a selected candidate (STox15) encoding a newly identified domain showed that it is an antibacterial effector belonging to the NlpC/P60 superfamily with a permuted catalytic core. STox15 displays phospholipase activity *in vitro* and its ectopic expression in target cells modifies the membrane composition. This study offers a comprehensive characterization of new toxins, especially the arsenal linked to T6SSs in *Salmonella*, identifying novel effector families and providing an in-depth analysis of a new protein family that specifically targets lipids.

Results

Identification of the T6SS toxin repertoire within 10,000 *Salmonella* genomes

T6SS effectors are often encoded in close genomic proximity to structural components of the system[16,20,21]. To identify new effectors, we employed a "guilt-by-association" approach, which relies on the conservation of genomic context and is a powerful strategy for pinpointing new effectors[22]. We applied this methodology to a dataset of *Salmonella* genomes (10KSG)[23] (Fig. 1A). First, we located and classified the T6SS clusters using hidden Markov models (HMMs) from different sources[9,24-26]. We collected 10 genes upstream and downstream of each locus encoding T6SS components, referred to as genomic sites (Fig. 1A). A total of 42,560 genomic sites housing at least one T6SS component were identified. We then applied a graph theoretic strategy leveraging the Jaccard index for network construction[27], followed by the Louvain algorithm[28] to automatically categorize genomic sites. Analysis resulted in five categories: T6SS subtype i1, i2, i3, i4b, and orphan (Fig. 1A). Interestingly, we observed mobility of the distinct subtypes among genomic sites and pathogenicity islands, depending on the strain and/or serovar. Using tRNAs as markers to identify the insertion sites[29], we found that subtype i3 (90%, 4929/5461 genomic sites) is mainly located within SPI-6 and flanked by the aspartate tRNA ($tRNA^{Asp}$)[16], while subtype i1 is not well conserved and found within SPI-19 associated with $tRNA^{Ala}$ (12%, 66/532 genomic sites)[16], and SPI-6 (3%, 18/532 genomes) flanked by $tRNA^{Asp}$ - most subtype i1 could not be assigned to a specific location (82%, 437/532 genomic sites). These results indicate that distinct T6SSs subtypes are inserted into different genomic sites that are hot spots for horizontal transfer events, and the combination between the insertion site and the introduced subtype varies according to the *Salmonella* strain and serovar.

Next, we focused on identifying toxins using three strategies (Fig. 1D). First, we located proteins containing N-terminal PAAR, VgrG and Hcp domains and additional C-terminal domains with more than 50 amino acids. These C-terminal regions were isolated and grouped (80% coverage and 1e-3 e-value). Second, we used the genomic sites containing T6SS components and analyzed up to five genes upstream and downstream via the software BastionX[30]. Third, we used amino acid sequences, HMMs and PSSMs (position-specific scoring matrix) from SecReT6[31], Pfam[25], and Zhang, et al. [9] to search the 10KSG dataset for previously described effectors. For candidates not recognized by previously described models, we collected homologs from NCBI using 4 iterations of PSI-BLAST[32] and generated multiple sequence alignments and HMMs. We then used a series of sequence and structure-based strategies to classify and annotate the function of these candidates: i) profile-profile comparison methods such as HHsearch[33] were used to detect distant homologs; ii) structural models were created using Alphafold2[34] from multiple sequence alignments to perform searches in FoldSeek[35] and DALI[36] against PDB[37] and AlphaFoldDB[38]; iii) the structure-structure comparison algorithm from FoldSeek was used to cluster groups of candidates. All information collected was manually examined to establish the final domain annotation (Fig. 1D). Candidates that displayed sequence or structural similarity to known toxin domains or proteins of unknown function that displayed conserved genomic organization and/or adjacent conserved putative immunity proteins across several species were maintained.

In total, we identified 128 groups of toxins (Table S1 and Fig. 1F). Eighty-three were already described in public databases (e.g. Ntox47)[9,25], or represent individual effectors that were experimentally characterized but for which HMMs have not been produced and made available (e.g. TreTu)[21,39-54]. For the latter, the newly created HMMs were named with a ".st" suffix (e.g. TreTu.st). In addition, 45 groups comprise

new toxin domains or highly divergent variations that were not detected by previously published HMMs (Fig. 1E). This justified them being distinct groups requiring the design of new HMMs. These groups of effectors were named STox followed by a number (e.g. STox_1) (Table S1 and Fig. 1F). It is worth noting that these toxin domains are widespread across several species and constitute polymorphic toxin domains[9]. A few examples of species encoding each STox, together with the amino acid sequence alignments and AlphaFold prediction can be found at https://leepbioinfo.github.io/10ksgt6ss.

Inspection of genomic context across several bacterial species revealed that most candidates exhibited a conserved adjacent gene coding for a predicted immunity protein, thus suggesting antibacterial activity (83.6%, 107/128). Some effectors, which lacked conserved immunity proteins, were predicted to display anti-eukaryotic activity (12.4%, 14/128) (Table S1 and Fig. 1F). The analysis revealed a diverse array of cellular targets and biochemical activities among the 128 toxin groups (Table S1 and Fig. 1F). Notably, the activities of a few STox effectors could not be predicted confidently and will require further analysis (Fig. 1F). Overall, these findings highlight the significant diversity of toxins encoded by *Salmonella* and reveal an array of effectors used in interbacterial competition and as virulence factors throughout a diverse array of bacterial lineages.

Salmonella serovars encode diverse sets of toxins with target-specific activities

After classifying the subtypes and carefully identifying the effectors within the 10KSG dataset, we estimated the average number of effectors per genome to be 3.57 ± 1.42 for genomes encoding one T6SS cluster (Fig. 2A, blue), and 5.35 ± 2.42 effectors

for genomes containing two clusters (Fig. 2A, orange). It is worth highlighting that our manual curation was very stringent, so these numbers might be underestimated.

The most frequent effectors detected within the dataset were the peptidoglycan-targeting Tlde1[20] and Tae4[39]; followed by RNases Ntox47[55]; the metallopeptidase Tox-HopH1; and ADP-ribosyltransferases TreTu[40] and STox_62 (Fig. 2B). Together, these toxin domains constitute the core effectors in the 10KSG dataset. Next, we determined the 5 most frequent effectors detected in each of the 149 *Salmonella* serovars (Fig. 1C and Fig. S2). Serovars that predominantly encode subtype i3 harbor predominantly antibacterial effectors, while serovars containing subtype i1 lack toxins targeting the peptidoglycan and show toxins with anti-eukaryotic activity, such as peptidases and pore-forming proteins (Fig. 2C). The core effectors of each serovar can be found in Fig. S2. This data supports the classification of *Salmonella* T6SS subtype i3 as antibacterial and subtype i1 as anti-eukaryotic (Fig. 2E). Notably, effectors encoded within or close to T6SS structural clusters, show minimum overlap (Fig. 2F), thus suggesting an evolutionary scenario where T6SS clusters are acquired alongside with associated set of effectors and/or that certain subsets of effectors are preferably exchanged among bacteria harboring similar T6SS subtypes.

Previous analysis of subtype i3 identified the insertion of three variable regions between the structural genes (VR1-3) in which effectors are encoded[16] (Fig. 2G). Our results indicate that VR1 and VR2 contain mainly toxins targeting the periplasm (e.g. Tae2, Tae4, Tlde1, STox_15) whereas VR3 primarily houses toxins targeting the cytoplasm (e.g. Ntox47, Tox-WHH, TreTu). The latter are typically associated with an N-terminal PAAR domain and Rhs (Rearrangement hotspot) repeats, which assist in the translocation across the bacterial inner membrane to reach the cytoplasmic targets[40,55-57] (Fig. 2G). The position of effectors at the edge of the T6SS cluster and the domain

architecture containing Rhs repeats facilitate recombination events[55], leading to the greater diversity of effectors observed at the VR3 (Fig. S1).

STox15 has a permuted NlpC/P60 domain and is evolutionarily related to enzymes targeting lipids

Among the newly identified toxins, STox15 emerged as one of the most abundant (Fig. 2B). To analyze whether STox15 and its associated downstream gene (SImm15) form an effector and immunity pair, we cloned these genes in compatible vectors under the control of different promoters and assessed toxicity upon expression in *Escherichia coli*. STox15 is toxic in the periplasm but not in the cytoplasm of *E. coli* and co-expression with SImm15 neutralizes the effect (Fig. 3B). Next, we performed time-lapse microscopy to evaluate bacterial growth and morphology at the single cell level. *E. coli* carrying the plasmid with SP-STox15 grew normally in d-glucose (repressed conditions) (Movie S1); however, shortly after induction of SP-STox15 with l-arabinose, cells began lysing (Movie S2). It was curious that cells lysed without losing their rod shape, which suggests that the peptidoglycan was not affected (Fig. 3C). After lysing, residual structures resembling the intact peptidoglycan sacculus remained (Fig. 3C), indicating that this is not the target of STox15. In addition, we noticed that the cognate immunity protein SImm15 contains a conserved domain with two transmembrane helices (Fig. S3), suggesting that the site of its neutralizing action occurs at the cell membrane.

Although the STox15 domain was not identified by any of the HMMs deployed in the initial steps of this study, subsequent HHpred analysis revealed a significant probability of homology with DUF4105 and the effector TseH from *Vibrio cholerae*[45] (data not shown), both of which are members of the NlpC/P60 superfamily[58,59]. This

superfamily was previously defined as encompassing four families, which are divided into two higher-order groups (canonical and permuted)[58]. Members of the canonical group (AcmB-like and P60-like) function as peptidases involved in peptidoglycan hydrolysis[60], while permuted members (YaeF-like and LRAT-like) exhibit a circular permutation in their catalytic core, creating a hydrophobic binding pocket that provides specificity for lipids[61,62]. Closer inspection of the sequence and structure of STox15 revealed a circular permutation of the catalytic domain indicating that it belongs to the permuted NlpC/P60 group (https://leepbioinfo.github.io/10ksgt6ss/)[58].

To predict the function of STox15, we sought to understand its evolutionary relationship by constructing a phylogenetic tree using the sequences of STox15, TseH and additional permuted members, such as LRAT and YiiX. The analysis revealed the formation of five major clades including YiiX, LRAT, TseH, STox15 and DUF4105 (Fig. 3D, Table S2 and Table S3). Genomic context analysis predicted that proteins of the STox15 clade are toxins deployed in biological conflicts (Fig. 3D and 3E). Similarly, the TseH clade (Pfam DUF6695) displays genomic contexts indicative of biological conflicts (Fig. 3D and 3E). The clades LRAT and YiiX harbor proteins known to be involved in lipid metabolism: LRAT (lecithin:retinol acyltransferase) is an enzyme present in mammals and involved in the transference of acyl groups from phosphatidylcholine to all-trans retinol to produce all-trans retinyl esters that are storage forms of vitamin A[63]; H-RAS-like suppressor (HRASLS) proteins are a group within the LRAT family that display both acyltransferase and phospholipase A1/2 activities[64]; and YiiX-like family members from *Bacillus cereus* are active against lipids[62].

Interestingly, STox15 emerged as the sister clade of DUF4105 (Fig. 3D and 3E). Our comparative genomics analysis revealed a recurring evolutionary pattern in which DUF4105 domain-containing proteins are repeatedly displaced by apolipoprotein N-

acyltransferases (Lnt) across three distinct genomic contexts (Fig. 3E). Hence, we proposed that DUF4105 could be working as an acyltransferase. Remarkably, DUF4105 was recently identified as the missing lipoprotein N-acyltransferase in *Bacteroides*[65], which was named Lnb (N-acyltransferase in *Bacteroides*). These experimental results confirmed our independent *in-silico* prediction for the function of DUF4105 and provide two different lines of evidence leading to similar conclusions. It is noteworthy that the DUF4105 clade identified in our analysis consists primarily, though not exclusively, of *Bacteroides* species, with a branch enriched in Gram-positives like *Firmicutes* (Fig. 3D). The list of homologs containing DUF4105 can be found in Table S3C and S3D.

Multiple sequence alignments of each of the permuted clades including STox15 revealed the conserved catalytic His and Cys residues characteristic of the NlpC/P60 superfamily (Fig. 3F)[58]. Substitution of these residues for alanine ($STox15_{H43A}$ and $STox15_{C151A}$) eliminated toxicity in *E. coli* (Fig. 3G). These findings collectively confirm that the enzymatic function of the NlpC/P60 papain-like fold domain is crucial for toxicity. Collectively, the periplasmic-acting phenotype of STox15, the presence of a membrane-associated immunity protein and the fatty acyl linkage targeting activities common in the permuted NlpC/P60 members strongly support a function for STox15 in targeting membrane lipids.

STox15 displays phospholipase activity and changes the membrane composition of intoxicated cells

To analyze the enzymatic activity of STox15, we incubated purified recombinant protein (Fig. S4) with either purified phosphatidylglycerol (PG) 16:0-18:1 or phosphatidylethanolamine (PE) 16:0-18:1 and analyzed the reaction product by HPLC

coupled to mass spectrometry (Fig. 4A and B). Results showed that STox15 has predominantly phospholipase A1 activity and cleaves both PG and PE (a preference for cleaving off the 16:0 acyl chain) as observed by the accumulation of 18:1 lysophospholipids (Fig. 4A and B).

Next, we set out to determine whether STox15 could cause changes in the composition of phospholipids when ectopically expressed by target cells. *E. coli* harboring the pBRA SP-STox15 plasmid were grown to OD_{600nm} of 1.0 in the presence of d-glucose (repressed), washed and resuspended in AB medium with l-arabinose to induce the expression of the toxin. Total lipids were extracted and analyzed by UHPLC-MS. We observed a general decrease in intact phospholipid forms in $STox15_{WT}$, especially phosphatidylglycerol (PG), when compared with the catalytic mutant $STox15_{C151A}$ (Fig. 4A and 4B). In addition, an increase in lysophospholipids forms - either lysophosphatidylglycerol (LPG) or lysophosphatidylethanolamine (LPE) - and free fatty acids (FFA) was detected in the wild-type (Fig. 4A and 4B). Lysophospholipids possess amphiphilic properties and have an inverted cone-shaped molecular structure that interacts with and modifies membrane properties (e.g. curvature) similarly to detergents[66]. The accumulation of lysophospholipids on the target cell membrane likely promotes the observed membrane disruption (Fig. 3C) due to its detergent-like properties[67]. Collectively, these results confirm that STox15 targets phospholipids similarly to other proteins possessing a permuted NlpC/P60 domain, and that STox15 displays phospholipid-degrading activity. It remains to be determined whether STox15 also possesses acyltransferase activity as reported for other permuted NlpC/P60.

Discussion

Our comprehensive analysis of 10,000 *Salmonella* genomes has significantly expanded the repertoire of polymorphic toxins, identifying 128 candidates, including 45 novel toxin domains. Our study employed a robust bioinformatic pipeline, integrating classical methods with the latest structural bioinformatics techniques. The combination of sensitive sequence and structure searches with comparative genomics provided a comprehensive understanding of the identified toxin domains. In addition, the manual curation of candidates ensured high confidence in our results, distinguishing our approach from previous large-scale *in-silico* analyses. The identification of these novel toxin domains builds upon the foundational work by Zhang et al.[9] and others[30,68-76], which characterized the diversity of polymorphic toxin systems across bacterial lineages. The identification of novel toxin domains highlights the constant evolutionary arms race between bacteria, driving the diversification of toxin and immunity proteins.

This study not only broadens our understanding of toxin domains but also provides the first direct characterization of a lipid-targeting NlpC/P60 domain. The phospholipase activity of STox15, which cleaves acyl groups from phosphatidylglycerol and phosphatidylethanolamine, underscores its role in membrane disruption during bacterial competition. Interestingly, our phylogenetic analysis revealed an evolutionary link between STox15 and a new family of lipoprotein N-acyltransferases in *Bacteroides*, adding a new dimension to the functional diversity of these toxins. Notably, one of the homologs of STox15 is TseH[45,77], which has been proposed to be an endopeptidase due to its NlpC/P60 domain and similarity to the amidase Tse1[78,79]. However, unlike Tse1, TseH exhibits a permutation in its catalytic core[77]. This permutation, along with its evolutionary relationship to STox15 and other permuted NlpC/P60, suggests that TseH actual substrate might be an acyl group in phospholipids rather than a peptide/amide bond. Exploring the potential acyltransferase activity of

STox15 and its homologs could reveal further biochemical diversity within the NlpC/P60 superfamily.

In the context of *Salmonella* biology, the unprecedented diversity of T6SS effectors presents numerous opportunities for new studies. Our findings reveal the existence of a core repertoire of T6SS effectors for each serovar, suggesting that *Salmonella* acquire and maintain effectors in response to specific environmental pressures and contexts rather than accumulating an increasingly larger array of effectors. Notably, we observed a higher number of effectors in serovars isolated from environmental sources compared to those from patients, indicating that the number of effectors increases in more diverse environments where there are potentially more encounters with a variety of competitor species.

In conclusion, our comprehensive analysis has greatly enhanced the understanding of toxins involved in bacterial competition and pathogenesis. The identification of previously uncharacterized toxin domains highlights the potential for discovering novel biochemical activities. This study provides a solid foundation for future research into the complex dynamics of conflict systems and their implications for bacterial ecology and pathogenesis.

Methods

Comparative genomic analysis

The .gff files from the genome assemblies retrieved from the 10KSG project[23] were organized and stored in tabular format using Python scripts, based on the Biopython[80] and pandas[81] libraries. Iterative searches were conducted using Jackhmmer[82] with a 10e-6 e-value cutoff. Protein clustering was performed using MMseqs[83] to remove redundancy (80% coverage and 70% identity) and form

homologous groups (80% coverage and e-value 10e-3). Multiple sequence alignments were generated using the local-pair algorithm in MAFFT[84], and phylogenetic trees were constructed using FastTree[85]. Domain identification and annotation was performed using HMMsearch and HMMscan[82,86] and models from the databases Pfam[25], TXSScan[24], and BastionHub[87]. Remote homology identification was performed using HHpred[33] and FoldSeek.

Bacterial strains

A list of bacterial strains used in this work can be found in Table S4. Strains were grown at 37 °C in Lysogeny Broth (10 g/L tryptone, 10 g/L NaCl, 5 g/L yeast extract) under agitation. AB medium was used for lipidomics: 0.2% (NH4)2SO2, 0.6% Na2HPO4, 0.3% KH2PO4, 0.3% NaCl, 0.1 mM CaCL2, 1 mM MgCl2, 3 µM FeCL3, supplemented with 0.2% sucrose, 0.2% casamino acids, 10 µg/mL thiamine, and 25 µg/mL uracil. Cultures were supplemented with antibiotics in the following concentration when necessary: 50 µg/mL kanamycin, 100 µg/mL ampicillin, and 50 µg/mL streptomycin.

Cloning and mutagenesis

All primers are listed in Table S4. STox15 and SImm15 were amplified by PCR and cloned into pBRA vector under the control of P_{BAD} promoter[88] with or without pelB signal peptide sequence from pET22b (Novagen)[89]. SImm15 was cloned into pEXT22 under the control of P_{TAC} promoter[90]. For protein expression and purification, STox15 was cloned into pET28a (Novagen), including a C-terminal Strep II tag. Point mutations ($STox15_{H43A}$, $STox15_{C151A}$) were created using QuikChange II XL Site-Directed

Mutagenesis Kit (Agilent Technologies) or by splicing by overlap extension (SOE) PCR. All constructs were confirmed by sequencing.

E. coli toxicity assay

Overnight cultures of *E. coli* DH5α co-expressing effectors for cytoplasmic (pBRA-STox15) or periplasmic (pBRA SP-STox15) localization and immunity protein (pEXT22-SImm15) were adjusted to OD_{600nm} 1, serially diluted in LB (1:4) and 5 µL were spotted onto LB agar (1.5%) containing either 0.2% d-glucose or 0.2% l-arabinose plus 200 µM IPTG, supplemented with streptomycin and kanamycin, and incubated at 37°C for 20 h.

Time-lapse microscopy

For time-lapse microscopy, LB agar (1.5%) pads were prepared by cutting a rectangular piece out of a double-sided adhesive tape, which was taped onto a microscopy slide as described previously[89]. *E. coli* DH5α harboring pBRA SP-STox15 was subcultured in LB (1:50) with 0.2% d-glucose until reaching OD_{600nm} 0.4–0.6 and adjusted to OD_{600nm} 1. Cultures were spotted onto LB agar pads supplemented either with 0.2% d-glucose or 0.2% l-arabinose plus antibiotics. Images were acquired every 15 min for 16 hr using a Leica DMi-8 epifluorescent microscope fitted with a DFC365 FX camera (Leica) and Plan-Apochromat ×63 oil objective (HC PL APO ×63/1.4 Oil ph3 objective Leica). Images were analyzed using FIJI software (Schindelin et al., 2012).

Protein expression and purification

E. coli BL21(DE3) carrying pET28a STox15$_{WT}$-Strep or STox15$_{C151A}$-Strep were grown in 4 L of LB supplemented with kanamycin (37 °C, 180 rpm) until OD_{600nm} 0.7. Expression was induced with 1 mM IPTG for 16 hr at 16 °C. Cells were harvested via centrifugation at 5000 *g* for 20 min, and pellets were resuspended in lysis buffer (50 mM Tris HCl pH 8.0, 350 mM NaCl, 45 mM β-mercaptoethanol, 5 mg/mL lysozyme, 10% glycerol) and lysed at 4°C using a sonicator. The lysate was centrifuged at 40,000 *g* for 45 min at 4°C. The supernatant was loaded onto a 1 ml StrepTrap HP column (Cytiva) equilibrated in buffer (50 mM Tris-HCl pH 8.0, 350 mM NaCl, 10% glycerol). The column was washed with 40 column volumes (CV) of wash buffer (50 mM Tris-HCl pH 8.0, 1 M NaCl, 10% glycerol, 45 mM β-mercaptoethanol), followed by a second wash with 12 CV (50 mM Tris-HCl pH 8.0, 1.5 M urea) to remove chaperonin GroEL[91]. The column was subjected to a third round of washes with 40 CV of wash buffer and eluted with 10 CV of elution buffer (50 mM Tris-HCl pH 8.0; 350 mM NaCl; 10% glycerol; 50 mM biotin). Fractions were buffer exchanged (25mM Tris-HCl pH 7.5, 100 mM NaCl, 5% glycerol) and concentrated using an Amicon of 30 kDa (Sigma). Protein aliquots were snap-frozen until use.

In vitro **phospholipase assay**

For *in vitro* enzymatic assay, phospholipids 1-palmitoyl-2-oleoyl-sn-glycero-3-phospho-(1'-rac-glycerol) (PG 16:0-18:1) and 1-palmitoyl-2-oleoyl-sn-glycero-3-phosphoethanolamine (PE 16:0-18:1) were purchased from Avanti Polar Lipids. Substrates were resuspended and diluted in methanol to adjust the concentration of aliquots. The methanol of each aliquot was dried under a nitrogen flow. A total of 1.2 mM of phospholipids (PG or PE) were resuspended in reaction buffer (25 mM Tris-HCl pH 7.5, 100 mM NaCl, 0.5 mM $CaCl_2$, 0.5 mM $MgCl_2$, 180 mM sodium deoxycholate

and 0.5 mM DTT) and incubated with 0.8 mM of enzyme ($STox15_{WT}$ or $STox15_{C151A}$) in a total volume of 100 µL for 2 h at 37°C under agitation (350 rpm). Lipids were extracted by adding 830 µL of a mixture of MTBE/methanol/water (10:3:2.5, v/v/v), followed by incubation under agitation for 1 h at room temperature. Samples were centrifuged for 2 min at 220 *g* and 350 µL of the top fraction was transferred to a new tube, dried in a SpeedVac and stored at –80 °C until analysis.

For mass spectrometry analysis, samples were resuspended in 350 µL of isopropanol and analyzed in a Shimadzu 8060 Triple Quadrupole Liquid Chromatograph Mass Spectrometer. Samples (0.1-0.5 µL) were loaded into an Agilent column C18 ZORBAX Eclipse Plus (4.6 x 150 mm, 5 µm, 400 bar) with a flow rate of 0.5 mL/min and an oven temperature of 40 °C. HPLC gradients were as described below for lipidomic analysis. The phospholipids and lysophospholipids of interest were analyzed in the multiple reaction monitoring (MRM) mode using m/z transitions, collision energies (CE) and dwell times as shown in Table S5A. Data was acquired by Shimadzu LabSolutions and processed in LabSolutions Browser. Graphs were plotted using GraphPrism 5.

Lipidomics of STox15-intoxicated *E. coli*

E. coli MG1655 containing the plasmids pBRA SP-$STox15_{WT}$ or SP-$STox15_{C151A}$ were cultured in LB containing 0.2% d-glucose at 37 °C for 14 h. Cells were subcultured in LB 0.2% d-glucose until an OD_{600nm} of 1 and centrifuged (10 min, 2900 *g*, 30 °C). Cells were washed with 40 mL of preheated AB medium at 37 °C, centrifuged (10 min, 2900 *g*, 30 °C), and resuspended in 5 mL of AB supplemented with 0.2% l-arabinose to induce STox15 expression. Cells were incubated for 1 h at 37 °C with agitation (100 rpm). The cells were centrifuged (15 min, 2900 *g*, 4 °C) and

washed once with 1 mL of PBS pH 7.4. PBS was removed by centrifugation and the cell pellet was stored at -80 °C until lipid extraction. A cocktail of class specific internal standards was added to the cell mass prior to lipid extraction for subsequent quantification and normalization (Table S5B). Total lipid extraction was performed using an adapted version of the protocol described by Yoshida, et al. [92]. Briefly, cell pellets were resuspended with 500 µL of cold methanol and 1 mL of MilliQ water and transferred to glass tubes. A mixture of chloroform and ethyl acetate (4:1) was added, followed by agitation for 1 min at 25 °C. Samples were centrifuged (2 min, 1500 *g*, 4 °C) and the lipid-containing phase (lower phase) was extracted and transferred to a new glass tube that was dried under a nitrogen (N_2) flow until all solvent traces were evaporated. Samples were stored at -80 °C until analysis.

Lipid extracts were diluted in 100 µL of isopropanol and analyzed using ultra-high performance liquid chromatography (UHPLC Nexera, Shimadzu) coupled with an ESI-Q-TOF mass spectrometer (Triple TOF 6600, Sciex) (UHPLC-Q-TOF/MS). 2 µL of each sample were injected into the UHPLC-MS, and molecules were separated using a CORTECS column (C18, 1.6 µm, 2.1x100 mm, Waters) with a flow rate of 0.2 mL/min and temperature set to 35 °C [93]. The mobile phases consisted of (A) water/acetonitrile (60:40) and (B) isopropanol/acetonitrile/water (88:10:2). Ammonium acetate at a final concentration of 10 mM was incorporated in both mobile phases A and B for the negative ionization acquisition mode. The gradient elution used in the chromatography was from 40 to 100% (mobile phase) B over the first 10 min; 100% B from 10-12 min; 100 to 40% B for 12-13 and holding 40% B for 13-20 min. The negative mode was utilized for the examination of phospholipids and free fatty acids. MS and MS/MS data acquisition was performed using Analyst 1.7.1 software (Sciex). Mass spectrometry data was inspected using PeakView 2.0 software (Sciex), and lipid

molecular species were manually identified with the help of an in-house manufactured Excel-based macro. Lipid species were quantified using MultiQuant software (Sciex), where the precursor ions areas were normalized by the internal standards for each class (Table S5B).

Data availability

All data supporting the findings of this study are available within the paper and its Supplementary Information files or at https://leepbioinfo.github.io/10ksgt6ss/. All data and code used for sequence and genome context analyses are available on a GitHub repository at https://github.com/leepbioinfo/10ksgt6ss. The ROTIFER package can be downloaded from the GitHub repository https://github.com/leepbioinfo/rotifer. The contents of both repositories are made available under the Creative Commons Attribution 4.0 International or the GNU Lesser General Public License (LGPL) v. 2.0. We have also uploaded the GitHub data and code to Zenodo (DOI: 10.5281/zenodo.13845778).

Author contributions

G.G.N., R.F.S. and E.B.-S. conceived the study; G.G.N., S.S.-S., T.W.C.S. and R.F.S. conducted bioinformatic analysis; S.S.-S., J.T.H., J.P.M., R.S.S. performed experiments and analyzed data; B.M.P.-S., S.M., L.A. analyzed data and contributed with discussions; G.G.N., R.F.S. and E.B.-S. wrote the manuscript with input from the other authors.

Acknowledgments

We are grateful to Jay Hinton for initially sharing the 10KSG dataset with us, to Ian Riddington for assistance with mass-spectrometry analysis of phospholipids, and Gerd Prehna and Larissa Diniz for discussions about enzymatic assay. Marcos Yoshinaga from PinguisLab for lipidomic data processing. Edgar Llontop and Diorge Paulo Souza for troubleshooting with protein purification. Cristiano G. Moreira for sharing strains. Alexandre Bruni for access to the microscope. Luize Nobrega Silva and Gustavo Chagas for technical support. This research was supported by Sao Paulo Research Foundation grant #2017-02178-2 to E.B-S, #2013/07937-8 to S.M, #2016/09047-8 and # 2021/10577-0 to R.F.S and #2021/10577-0 to T.W.C.S. Startup funds from MBS and CNS to E.B-S. This research was supported in part by an appointment to the National Library of Medicine Research Participation Program administered by the Oak Ridge Institute for Science and Education (ORISE) through an interagency agreement between the U.S. Department of Energy (DOE) and the National Library of Medicine. ORISE is managed by ORAU under DOE contract number DE-SC0014664. All opinions expressed in this paper are the author's and do not necessarily reflect the policies and views of NIH, NLM, DOE, or ORAU/ORISE. This work is supported by the funds of the Intramural Research Program of National Library of Medicine at the National Institutes of Health, USA (to L.A. and G.G.N). This work utilized the NIH HPC Biowulf computer cluster.

Competing interests

The authors declare no competing interests.

Figure legends.

Fig. 1: The T6SS effector repertoire within 10k *Salmonella* genomes.

(a) Pipeline used for classification of genomic sites and T6SS subtypes. **(b)** Number of genomes containing the different T6SS subtypes within the 10KSG dataset. **(c)** Examples of the genomic organization of T6SS structural clusters from distinct phylogenetic subtypes. **(d)** *In silico* strategies used for the identification and classification of T6SS effectors. **(e)** Comparison of profile Hidden Markov Models (pHMMs) of STox to published models of related families. Each circle corresponds to a population of proteins detected by an STox model. The relative frequency of proteins detected by an STox model compared to a reference model is shown on the horizontal axis. The HMM divergence score is shown in the vertical axis. The blue-white-red color scale of each dot represents the values for the Spearman correlation index between STox and reference alignment scores for the same proteins. Yellow circles represent STox models that detect proteins that are not recognized by previously existing models. The radius of each circle is proportional to the total number of proteins detected only by STox models. The regression line does not include the data points for the models represented by yellow circles. **(f)** Schematic representation of the functional classes of T6SS effector domains identified in the 10KSG distributed according to target cell type (see the complete list in Table S1).

Fig. 2: The diversity of *Salmonella* T6SS effectors and target-specific subsets.

(a) Normal distribution and fitted curve showing the number of effectors per genome (single cluster in blue and >2 clusters in orange). **(b)** The most frequent effectors identified in the 10KSG dataset. Each bar represents the number of genomes encoding a specific effector. Colors represent different biochemical activities, with light colors representing orphan effectors while dark colors represent effectors encoded within the structural cluster. **(c)** The five most frequent effectors encoded in different *Salmonella*

serovars (see Fig. S2 for all the 149 serovars). Colors indicate the effector activity as in (b). **(d)** Schematic representation of the most common sets of effectors in genomes encoding different T6SS subtypes. The number of genomes is indicated on the right. Colors represent activity as shown in (b). **(e)** Pie chart illustrating the relative proportions of effectors by activities encoded within the T6SS subtypes i3, i1, and i2. **(f)** Venn diagram illustrating the proportion of overlap between effectors encoded within each T6SS structural cluster (blue: i1; purple: subtype i2; red: subtype i3; and green: orphan). **(g)** Schematic representation of the genetic organization of T6SSs showing the position of variable regions in which the effector and immunity proteins are encoded. Colors denote structural proteins forming the membrane complex (orange), sheath and inner tube (light blue), baseplate and spike components (green). Effectors are shown in red, and immunities in dark blue.

Fig. 3: STox15 has a permuted NlpC/P60 domain that is required for toxicity.

(a) Scheme of the genomic region encoding STox15 and SImm15 effector/immunity pair (barcode FD01848827). **(b)** *E. coli* toxicity assay. Serial dilutions of *E. coli* carrying pBRA and pEXT22 constructs, as indicated, were spotted onto LB agar plates, and grown for 20 hr. Images are representative of three independent experiments. **(c)** Time-lapse microscopy of *E. coli* carrying pBRA SP-STox15 grown on LB agar pads containing either 0.2% d-glucose (repressed) or 0.2% l-arabinose (induced). Scale bar: 5 µm. Timestamps in hh:mm. **(d)** Maximum-likelihood phylogenetic tree of permuted NlpC/P60 members. Dots represent the number of PSI-BLAST iterations required to collect homologs and the red star marks the query: *S.* Oranienburg STox15 depicted in (a). **(e)** Genomic organization of representatives from clades TseH and STox15 showing the genes are encoded in the context of conflict systems, and DUF4105 showing context

of lipid metabolism. **(f)** Sequence logo from the enzymatic core of permuted NlpC/P60 from all clades shown in (d). The arrows indicate conserved His and Cys residues that were mutated in (g). **(g)** *E. coli* toxicity assay. Serial dilution of *E. coli* containing pBRA and pEXT22 constructs, as indicated, spotted onto LB agar plates and grown for 20 hr. Images are representative of three independent experiments.

Fig. 4: STox15 has phospholipase A activity and changes the composition of target cell membranes.

(a) *In vitro* enzymatic assay with recombinant STox15 (red) or STox15$_{C151A}$ (blue) incubated with different phospholipids (both 16:0-18:1 PG and PE) for 2 hr at 37 °C. The amount of lysophospholipids produced was analyzed and quantified by HPLC-MS/MS. **(b)** Quantification of the peak area of lysophospholipids normalized by the intact substrate. Data corresponds to the mean ± SD. ***$p < 0.001$ and *$p < 0.01$, *ns* not significant (Student's t-test). **(c)** UHPLC-MS total ion chromatogram showing the profile of total lipids extracted from *E. coli* expressing STox15 (red) or STox15$_{C151A}$ (blue). **(d)** Heatmap plot of top 20 altered lipids of intoxicated *E. coli* lipidome. Results display four biological replicates of each condition (WT or C151A) with the quantification of lipids species (Tukey test; $p < 0.05$ FDR adjusted). Data were expressed in nM mg of protein^{-1} and normalized by log transformation (base 10) prior to analysis. Red (up) and blue (down) bars represent changes in lipid species concentration relative to the normalized mean. Letters differentiate between the isomers.

Fig. S1: T6SS effector repertoire in the 10KSG dataset. Each column indicates the presence or absence of a toxin as identified by the models developed in this study. Lines denote unique combinations of effectors. The histogram on the right shows the

596 frequency of genomes in the 10KSG dataset containing each specific repertoire. The
597 histogram at the bottom illustrates the frequency of genomes with at least one protein
598 identified by the above HMM model. Effector activities are color-coded as described in
599 Fig. 2B.
600
601 **Fig. S2: List of five most frequent T6SS effectors identified in each of the 149**
602 ***Salmonella*** **serovars contained in the 10KSG dataset.** Colors indicate the effector
603 activity as in Fig. 2B.
604
605 **Fig. S3: SImm15 is a two-transmembrane helices protein. (a)** Sequence alignment of
606 SImm15 homologs with orange rectangles indicating predicted transmembrane helices.
607 Sequences are colored according to the Clustal X color scheme[94]. Consensus
608 abbreviations: h, hydrophobic (A, C, F, I, L, M, V, W, Y); l, aliphatic (L, I, V); a,
609 aromatic (F, W, Y); b, large residues (L, I, Y, E, R, F, Q, K, M, W); s, small residues
610 (A, G, S, V, C, D, N); u, tiny residues (G, A, S); p, polar residues (S, T, E, D, K, R, N,
611 Q, H, C); c, charged residues (D, E, H, K, R); +, positively charged residues (H, K, R);
612 −, negatively charged residues (D, E). (B) Transmembrane helix prediction for SImm15
613 using DeepTMHMM[95].
614
615 **Fig. S4: Recombinant protein purification used in enzymatic assay.** SDS–PAGE of
616 recombinant proteins during purification steps to obtain purified protein for enzymatic
617 assays. Affinity chromatography using Strep-Tactin sepharose to purify STox15
618 versions with C-terminus Strep-tag II: WT in (a) or C151A in (b). Recombinant proteins
619 were purified from the soluble fraction. An additional step of washing with 1.5M urea
620 was performed after the traditional washes to remove contamination with GroEL before

elution with biotin. Additional bands were identified by mass-spectrometry to confirm identity. MK: marker; INS: insoluble; SOL: soluble; FT: flowthrough. GroEL: chaperonin GroEL; Bccp: biotin carboxyl carrier protein; OmpF: outer membrane porin F.

Table S1. List of all T6SS toxin domains identified in this study in the 10K *Salmonella* genomes dataset.

Table S2. List of all homologs collected by JackHMMER searches and used to build the phylogenetic tree shown in Fig. 3D.

Table S3. Genomic context of members of each permuted NlpC/P60 members shown in Fig. 3D.

Table S4. List of strains, plasmids and primers used in the study.

Table S5. (a) MRM transition for LC-MS/MS method of lysophospholipids. (b) Internal standards used for lipidomics analysis in negative mode.

Movie S1. Time-lapse microscopy of *E. coli* harboring pBRA SP-STox15 growing in media supplemented with 0.2% d-glucose. Timestamp in hh:mm. Scale bar: 5 μm.

Movie S2. Time-lapse microscopy of *E. coli* harboring pBRA SP-STox15 growing in media supplemented with 0.2% l-arabinose. Timestamp in hh:mm. Scale bar: 5 μm.

References

1 Granato, E. T., Meiller-Legrand, T. A. & Foster, K. R. The Evolution and Ecology of Bacterial Warfare. *Curr Biol* **29**, R521-R537 (2019). https://doi.org/10.1016/j.cub.2019.04.024

2 Hood, R. D., Peterson, S. B. & Mougous, J. D. From Striking Out to Striking Gold: Discovering that Type VI Secretion Targets Bacteria. *Cell host & microbe* **21**, 286-289 (2017). https://doi.org/10.1016/j.chom.2017.02.001

3 Russell, A. B. *et al.* A type VI secretion-related pathway in Bacteroidetes mediates interbacterial antagonism. *Cell host & microbe* **16**, 227-236 (2014). https://doi.org/10.1016/j.chom.2014.07.007

4 Li, J. *et al.* SecReT6: a web-based resource for type VI secretion systems found in bacteria. *Environ Microbiol* **17**, 2196-2202 (2015). https://doi.org/10.1111/1462-2920.12794

5 Bock, D. *et al.* In situ architecture, function, and evolution of a contractile injection system. *Science* **357**, 713-717 (2017). https://doi.org/10.1126/science.aan7904

6 Boyer, F., Fichant, G., Berthod, J., Vandenbrouck, Y. & Attree, I. Dissecting the bacterial type VI secretion system by a genome wide in silico analysis: what can be learned from available microbial genomic resources? *BMC Genomics* **10**, 104 (2009). https://doi.org/10.1186/1471-2164-10-104

7 Barret, M., Egan, F., Fargier, E., Morrissey, J. P. & O'Gara, F. Genomic analysis of the type VI secretion systems in Pseudomonas spp.: novel clusters and putative effectors uncovered. *Microbiology (Reading)* **157**, 1726-1739 (2011). https://doi.org/10.1099/mic.0.048645-0

8 Hood, R. D. *et al.* A type VI secretion system of Pseudomonas aeruginosa targets a toxin to bacteria. *Cell host & microbe* **7**, 25-37 (2010). https://doi.org/10.1016/j.chom.2009.12.007

9 Zhang, D., de Souza, R. F., Anantharaman, V., Iyer, L. M. & Aravind, L. Polymorphic toxin systems: Comprehensive characterization of trafficking modes, processing, mechanisms of action, immunity and ecology using comparative genomics. *Biol Direct* **7**, 18 (2012). https://doi.org/10.1186/1745-6150-7-18

10 Cherrak, Y. *et al.* Biogenesis and structure of a type VI secretion baseplate. *Nat Microbiol* **3**, 1404-1416 (2018). https://doi.org/10.1038/s41564-018-0260-1

11 Jana, B. & Salomon, D. Type VI secretion system: a modular toolkit for bacterial dominance. *Future Microbiol* **14**, 1451-1463 (2019). https://doi.org/10.2217/fmb-2019-0194

12 Allsopp, L. P. & Bernal, P. Killing in the name of: T6SS structure and effector diversity. *Microbiology (Reading)* **169** (2023). https://doi.org/10.1099/mic.0.001367

13 Bohnhoff, M., Drake, B. L. & Miller, C. P. Effect of streptomycin on susceptibility of intestinal tract to experimental Salmonella infection. *Proc Soc Exp Biol Med* **86**, 132-137 (1954). https://doi.org/10.3181/00379727-86-21030

14 Rogers, A. W. L., Tsolis, R. M. & Baumler, A. J. Salmonella versus the Microbiome. *Microbiol Mol Biol Rev* **85** (2021). https://doi.org/10.1128/MMBR.00027-19

15 Sibinelli-Sousa, S., de Araujo-Silva, A. L., Hespanhol, J. T. & Bayer-Santos, E. Revisiting the steps of Salmonella gut infection with a focus on antagonistic interbacterial interactions. *FEBS J* (2021). https://doi.org/10.1111/febs.16211

16 Blondel, C. J., Jimenez, J. C., Contreras, I. & Santiviago, C. A. Comparative genomic analysis uncovers 3 novel loci encoding type six secretion systems differentially distributed in Salmonella serotypes. *BMC Genomics* **10**, 354 (2009). https://doi.org/10.1186/1471-2164-10-354

17 Bao, H. *et al.* Genetic diversity and evolutionary features of type VI secretion systems in Salmonella. *Future Microbiol* **14**, 139-154 (2019). https://doi.org/10.2217/fmb-2018-0260

18 Brunet, Y. R. *et al.* H-NS Silencing of the Salmonella Pathogenicity Island 6-Encoded Type VI Secretion System Limits Salmonella enterica Serovar Typhimurium Interbacterial Killing. *Infection and immunity* **83**, 2738-2750 (2015). https://doi.org/10.1128/IAI.00198-15

19 Sana, T. G. *et al.* Salmonella Typhimurium utilizes a T6SS-mediated antibacterial weapon to establish in the host gut. *Proceedings of the National Academy of Sciences of the United States of America* **113**, E5044-5051 (2016). https://doi.org/10.1073/pnas.1608858113

20 Sibinelli-Sousa, S. *et al.* A Family of T6SS Antibacterial Effectors Related to l,d-Transpeptidases Targets the Peptidoglycan. *Cell Rep* **31**, 107813 (2020). https://doi.org/10.1016/j.celrep.2020.107813

21 Hespanhol, J. T. *et al.* Antibacterial T6SS effectors with a VRR-Nuc domain are structure-specific nucleases. *Elife* **11** (2022). https://doi.org/10.7554/eLife.82437

22 Aravind, L. Guilt by association: contextual information in genome analysis. *Genome Res* **10**, 1074-1077 (2000). https://doi.org/10.1101/gr.10.8.1074

23 Perez-Sepulveda, B. M. *et al.* An accessible, efficient and global approach for the large-scale sequencing of bacterial genomes. *Genome Biol* **22**, 349 (2021). https://doi.org/10.1186/s13059-021-02536-3

24 Abby, S. S. *et al.* Identification of protein secretion systems in bacterial genomes. *Sci Rep* **6**, 23080 (2016). https://doi.org/10.1038/srep23080

25 Mistry, J. *et al.* Pfam: The protein families database in 2021. *Nucleic Acids Res* **49**, D412-D419 (2021). https://doi.org/10.1093/nar/gkaa913

26 Wang, J. *et al.* The conserved domain database in 2023. *Nucleic Acids Res* **51**, D384-D388 (2023). https://doi.org/10.1093/nar/gkac1096

27 Jaccard, P. The Distribution of the Flora in the Alpine Zone. *New Phytologist* **11**, 37-50 (1912). https://doi.org/10.1111/J.1469-8137.1912.TB05611.X

28 De Meo, P. F., E.; Fiumara, G.; Provetti, A. Generalized Louvain method for community detection in large networks. *International Conference on Intelligent Systems Design and Applications* (2011). https://doi.org/10.1109/ISDA.2011.6121636

29 Hansen-Wester, I. & Hensel, M. Salmonella pathogenicity islands encoding type III secretion systems. *Microbes and infection / Institut Pasteur* **3**, 549-559 (2001). https://doi.org/10.1016/s1286-4579(01)01411-3

30 Wang, J. *et al.* Bastion6: a bioinformatics approach for accurate prediction of type VI secreted effectors. *Bioinformatics* **34**, 2546-2555 (2018). https://doi.org/10.1093/bioinformatics/bty155

31 Zhang, J. *et al.* SecReT6 update: a comprehensive resource of bacterial Type VI Secretion Systems. *Sci China Life Sci* (2022). https://doi.org/10.1007/s11427-022-2172-x

32 Altschul, S. F. *et al.* Gapped BLAST and PSI-BLAST: a new generation of protein database search programs. *Nucleic Acids Res* **25**, 3389-3402 (1997). https://doi.org/10.1093/nar/25.17.3389

33 Soding, J., Biegert, A. & Lupas, A. N. The HHpred interactive server for protein homology detection and structure prediction. *Nucleic Acids Res* **33**, W244-248 (2005). https://doi.org/10.1093/nar/gki408

34 Jumper, J. *et al.* Highly accurate protein structure prediction with AlphaFold. *Nature* **596**, 583-589 (2021). https://doi.org/10.1038/s41586-021-03819-2

35 van Kempen, M. *et al.* Fast and accurate protein structure search with Foldseek. *Nat Biotechnol* **42**, 243-246 (2024). https://doi.org/10.1038/s41587-023-01773-0

36 Holm, L. Using Dali for Protein Structure Comparison. *Methods Mol Biol* **2112**, 29-42 (2020). https://doi.org/10.1007/978-1-0716-0270-6_3

37 Berman, H. M. *et al.* The Protein Data Bank. *Nucleic Acids Res* **28**, 235-242 (2000). https://doi.org/10.1093/nar/28.1.235

38 Varadi, M. *et al.* AlphaFold Protein Structure Database in 2024: providing structure coverage for over 214 million protein sequences. *Nucleic Acids Res* **52**, D368-D375 (2024). https://doi.org/10.1093/nar/gkad1011

39 Russell, A. B. *et al.* A widespread bacterial type VI secretion effector superfamily identified using a heuristic approach. *Cell host & microbe* **11**, 538-549 (2012). https://doi.org/10.1016/j.chom.2012.04.007

40 Jurenas, D. *et al.* Salmonella antibacterial Rhs polymorphic toxin inhibits translation through ADP-ribosylation of EF-Tu P-loop. *Nucleic Acids Res* **50**, 13114-13127 (2022). https://doi.org/10.1093/nar/gkac1162

41 Mariano, G. *et al.* A family of Type VI secretion system effector proteins that form ion-selective pores. *Nat Commun* **10**, 5484 (2019). https://doi.org/10.1038/s41467-019-13439-0

42 Hu, H. *et al.* Structure of the type VI secretion phospholipase effector Tle1 provides insight into its hydrolysis and membrane targeting. *Acta Crystallogr D Biol Crystallogr* **70**, 2175-2185 (2014). https://doi.org/10.1107/S1399004714012899

43 Bernal, P., Allsopp, L. P., Filloux, A. & Llamas, M. A. The Pseudomonas putida T6SS is a plant warden against phytopathogens. *ISME J* **11**, 972-987 (2017). https://doi.org/10.1038/ismej.2016.169

44 Miyata, S. T., Kitaoka, M., Brooks, T. M., McAuley, S. B. & Pukatzki, S. Vibrio cholerae requires the type VI secretion system virulence factor VasX to kill Dictyostelium discoideum. *Infection and immunity* **79**, 2941-2949 (2011). https://doi.org/10.1128/IAI.01266-10

45 Altindis, E., Dong, T., Catalano, C. & Mekalanos, J. Secretome analysis of Vibrio cholerae type VI secretion system reveals a new effector-immunity pair. *mBio* **6**, e00075 (2015). https://doi.org/10.1128/mBio.00075-15

46 Whitney, J. C. *et al.* Identification, structure, and function of a novel type VI secretion peptidoglycan glycoside hydrolase effector-immunity pair. *The Journal of biological chemistry* **288**, 26616-26624 (2013). https://doi.org/10.1074/jbc.M113.488320

47 Bullen, N. P. *et al.* An ADP-ribosyltransferase toxin kills bacterial cells by modifying structured non-coding RNAs. *Molecular cell* **82**, 3484-3498 e3411 (2022). https://doi.org/10.1016/j.molcel.2022.08.015

48 Li, D. Y. *et al.* Identification and Characterization of EvpQ, a Novel T6SS Effector Encoded on a Mobile Genetic Element in Edwardsiella piscicida. *Front Microbiol* **12**, 643498 (2021). https://doi.org/10.3389/fmicb.2021.643498

49 Berni, B., Soscia, C., Djermoun, S., Ize, B. & Bleves, S. A Type VI Secretion System Trans-Kingdom Effector Is Required for the Delivery of a Novel Antibacterial Toxin in Pseudomonas aeruginosa. *Front Microbiol* **10**, 1218 (2019). https://doi.org/10.3389/fmicb.2019.01218

50 Yahr, T. L., Vallis, A. J., Hancock, M. K., Barbieri, J. T. & Frank, D. W. ExoY, an adenylate cyclase secreted by the Pseudomonas aeruginosa type III system. *Proceedings of the National Academy of Sciences of the United States of America* **95**, 13899-13904 (1998). https://doi.org/10.1073/pnas.95.23.13899

51 Poole, S. J. *et al.* Identification of functional toxin/immunity genes linked to contact-dependent growth inhibition (CDI) and rearrangement hotspot (Rhs) systems. *PLoS Genet* **7**, e1002217 (2011). https://doi.org/10.1371/journal.pgen.1002217

52 Russell, A. B. *et al.* Diverse type VI secretion phospholipases are functionally plastic antibacterial effectors. *Nature* **496**, 508-512 (2013). https://doi.org/10.1038/nature12074

53 Koskiniemi, S. *et al.* Rhs proteins from diverse bacteria mediate intercellular competition. *Proceedings of the National Academy of Sciences of the United States of America* **110**, 7032-7037 (2013). https://doi.org/10.1073/pnas.1300627110

54 Jiang, F., Waterfield, N. R., Yang, J., Yang, G. & Jin, Q. A Pseudomonas aeruginosa type VI secretion phospholipase D effector targets both prokaryotic and eukaryotic cells. *Cell host & microbe* **15**, 600-610 (2014). https://doi.org/10.1016/j.chom.2014.04.010

55 Koskiniemi, S. *et al.* Selection of orphan Rhs toxin expression in evolved Salmonella enterica serovar Typhimurium. *PLoS Genet* **10**, e1004255 (2014). https://doi.org/10.1371/journal.pgen.1004255

56 Quentin, D. *et al.* Mechanism of loading and translocation of type VI secretion system effector Tse6. *Nat Microbiol* **3**, 1142-1152 (2018). https://doi.org/10.1038/s41564-018-0238-z

57 Ahmad, S. *et al.* Structural basis for effector transmembrane domain recognition by type VI secretion system chaperones. *Elife* **9** (2020). https://doi.org/10.7554/eLife.62816

58 Anantharaman, V. & Aravind, L. Evolutionary history, structural features and biochemical diversity of the NlpC/P60 superfamily of enzymes. *Genome Biol* **4**, R11 (2003). https://doi.org/10.1186/gb-2003-4-2-r11

59 Ozhelvaci, F. & Steczkiewicz, K. Identification and classification of papain-like cysteine proteinases. *The Journal of biological chemistry* **299**, 104801 (2023). https://doi.org/10.1016/j.jbc.2023.104801

60 Griffin, M. E., Klupt, S., Espinosa, J. & Hang, H. C. Peptidoglycan NlpC/P60 peptidases in bacterial physiology and host interactions. *Cell Chem Biol* **30**, 436-456 (2023). https://doi.org/10.1016/j.chembiol.2022.11.001

61 Golczak, M. *et al.* Structural basis for the acyltransferase activity of lecithin:retinol acyltransferase-like proteins. *The Journal of biological chemistry* **287**, 23790-23807 (2012). https://doi.org/10.1074/jbc.M112.361550

62 Xu, Q. *et al.* Structural analysis of papain-like NlpC/P60 superfamily enzymes with a circularly permuted topology reveals potential lipid binding sites. *PloS one* **6**, e22013 (2011). https://doi.org/10.1371/journal.pone.0022013

63 Sears, A. E. & Palczewski, K. Lecithin:Retinol Acyltransferase: A Key Enzyme Involved in the Retinoid (visual) Cycle. *Biochemistry* **55**, 3082-3091 (2016). https://doi.org/10.1021/acs.biochem.6b00319

64 Mardian, E. B., Bradley, R. M. & Duncan, R. E. The HRASLS (PLA/AT) subfamily of enzymes. *J Biomed Sci* **22**, 99 (2015). https://doi.org/10.1186/s12929-015-0210-7

65 Armbruster, K. M. *et al.* Identification and Characterization of the Lipoprotein N-acyltransferase in Bacteroides. *bioRxiv* (2024). https://doi.org/10.1101/2024.05.31.596883

66 Zheng, L., Lin, Y., Lu, S., Zhang, J. & Bogdanov, M. Biogenesis, transport and remodeling of lysophospholipids in Gram-negative bacteria. *Biochim Biophys Acta Mol Cell Biol Lipids* **1862**, 1404-1413 (2017). https://doi.org/10.1016/j.bbalip.2016.11.015

67 Henriksen, J. R., Andresen, T. L., Feldborg, L. N., Duelund, L. & Ipsen, J. H. Understanding detergent effects on lipid membranes: a model study of lysolipids. *Biophys J* **98**, 2199-2205 (2010). https://doi.org/10.1016/j.bpj.2010.01.037

68 Salomon, D. *et al.* Marker for type VI secretion system effectors. *Proceedings of the National Academy of Sciences of the United States of America* **111**, 9271-9276 (2014). https://doi.org/10.1073/pnas.1406110111

69 Jana, B., Fridman, C. M., Bosis, E. & Salomon, D. A modular effector with a DNase domain and a marker for T6SS substrates. *Nat Commun* **10**, 3595 (2019). https://doi.org/10.1038/s41467-019-11546-6

70 Fridman, C. M., Keppel, K., Gerlic, M., Bosis, E. & Salomon, D. A comparative genomics methodology reveals a widespread family of membrane-disrupting T6SS effectors. *Nat Commun* **11**, 1085 (2020). https://doi.org/10.1038/s41467-020-14951-4

71 Blondel, C. J., Amaya, F. A., Bustamante, P., Santiviago, C. A. & Pezoa, D. Identification and distribution of new candidate T6SS effectors encoded in Salmonella Pathogenicity Island 6. *Front Microbiol* **14**, 1252344 (2023). https://doi.org/10.3389/fmicb.2023.1252344

72 Kanarek, K., Fridman, C. M., Bosis, E. & Salomon, D. The RIX domain defines a class of polymorphic T6SS effectors and secreted adaptors. *Nat Commun* **14**, 4983 (2023). https://doi.org/10.1038/s41467-023-40659-2

73 Geller, A. M., Shalom, M., Zlotkin, D., Blum, N. & Levy, A. Identification of type VI secretion system effector-immunity pairs using structural bioinformatics. *Mol Syst Biol* **20**, 702-718 (2024). https://doi.org/10.1038/s44320-024-00035-8

74 Carobbi, A. *et al.* PIX is an N-terminal delivery domain that defines a class of polymorphic T6SS effectors in Enterobacterales. *Cell Rep* **43**, 114015 (2024). https://doi.org/10.1016/j.celrep.2024.114015

75 Jana, B., Keppel, K., Fridman, C. M., Bosis, E. & Salomon, D. Multiple T6SSs, Mobile Auxiliary Modules, and Effectors Revealed in a Systematic Analysis of the Vibrio parahaemolyticus Pan-Genome. *mSystems* **7**, e0072322 (2022). https://doi.org/10.1128/msystems.00723-22

76 Tchelet, D., Keppel, K., Bosis, E. & Salomon, D. Vibrio parahaemolyticus T6SS2 effector repertoires. *Gut Microbes* **15**, 2178795 (2023). https://doi.org/10.1080/19490976.2023.2178795

77 Hersch, S. J. *et al.* Envelope stress responses defend against type six secretion system attacks independently of immunity proteins. *Nat Microbiol* **5**, 706-714 (2020). https://doi.org/10.1038/s41564-020-0672-6

78 Russell, A. B. *et al.* Type VI secretion delivers bacteriolytic effectors to target cells. *Nature* **475**, 343-347 (2011). https://doi.org/10.1038/nature10244

79 Chou, S. *et al.* Structure of a peptidoglycan amidase effector targeted to Gram-negative bacteria by the type VI secretion system. *Cell Rep* **1**, 656-664 (2012). https://doi.org/10.1016/j.celrep.2012.05.016

80 Cock, P. J. *et al.* Biopython: freely available Python tools for computational molecular biology and bioinformatics. *Bioinformatics* **25**, 1422-1423 (2009). https://doi.org/10.1093/bioinformatics/btp163

81 McKinney, W. o. Data structures for statistical computing in python. . *Proceedings of the 9th Python in Science Conference* **445**, 51-56 (2010).

82 Johnson, L. S., Eddy, S. R. & Portugaly, E. Hidden Markov model speed heuristic and iterative HMM search procedure. *BMC Bioinformatics* **11**, 431 (2010). https://doi.org/10.1186/1471-2105-11-431

83 Hauser, M., Steinegger, M. & Soding, J. MMseqs software suite for fast and deep clustering and searching of large protein sequence sets. *Bioinformatics* **32**, 1323-1330 (2016). https://doi.org/10.1093/bioinformatics/btw006

84 Katoh, K. & Standley, D. M. MAFFT multiple sequence alignment software version 7: improvements in performance and usability. *Mol Biol Evol* **30**, 772-780 (2013). https://doi.org/10.1093/molbev/mst010

85 Price, M. N., Dehal, P. S. & Arkin, A. P. FastTree 2--approximately maximum-likelihood trees for large alignments. *PloS one* **5**, e9490 (2010). https://doi.org/10.1371/journal.pone.0009490

86 Eddy, S. R. Accelerated Profile HMM Searches. *PLoS computational biology* **7**, e1002195 (2011). https://doi.org/10.1371/journal.pcbi.1002195

87 Wang, J. *et al.* BastionHub: a universal platform for integrating and analyzing substrates secreted by Gram-negative bacteria. *Nucleic Acids Res* **49**, D651-D659 (2021). https://doi.org/10.1093/nar/gkaa899

88 Souza, D. P. *et al.* Bacterial killing via a type IV secretion system. *Nat Commun* **6**, 6453 (2015). https://doi.org/10.1038/ncomms7453

89 Bayer-Santos, E. *et al.* The opportunistic pathogen Stenotrophomonas maltophilia utilizes a type IV secretion system for interbacterial killing. *PLoS pathogens* **15**, e1007651 (2019). https://doi.org/10.1371/journal.ppat.1007651

90 Dykxhoorn, D. M., St Pierre, R. & Linn, T. A set of compatible tac promoter expression vectors. *Gene* **177**, 133-136 (1996). https://doi.org/10.1016/0378-1119(96)00289-2

91 Belval, L. *et al.* A fast and simple method to eliminate Cpn60 from functional recombinant proteins produced by E. coli Arctic Express. *Protein Expr Purif* **109**, 29-34 (2015). https://doi.org/10.1016/j.pep.2015.01.009

92 Yoshida, Y., Kodai, S., Takemura, S., Minamiyama, Y. & Niki, E. Simultaneous measurement of F2-isoprostane, hydroxyoctadecadienoic acid, hydroxyeicosatetraenoic acid, and hydroxycholesterols from physiological samples. *Anal Biochem* **379**, 105-115 (2008). https://doi.org/10.1016/j.ab.2008.04.028

93 Chaves-Filho, A. B. *et al.* Alterations in lipid metabolism of spinal cord linked to amyotrophic lateral sclerosis. *Sci Rep* **9**, 11642 (2019). https://doi.org/10.1038/s41598-019-48059-7

94 Larkin, M. A. *et al.* Clustal W and Clustal X version 2.0. *Bioinformatics* **23**, 2947-2948 (2007). https://doi.org/10.1093/bioinformatics/btm404

95 Hallgren, J. *et al.* DeepTMHMM predicts alpha and beta transmembrane proteins using deep neural networks. *bioRxiv*, 2022.2004.2008.487609 (2022). https://doi.org/10.1101/2022.04.08.487609

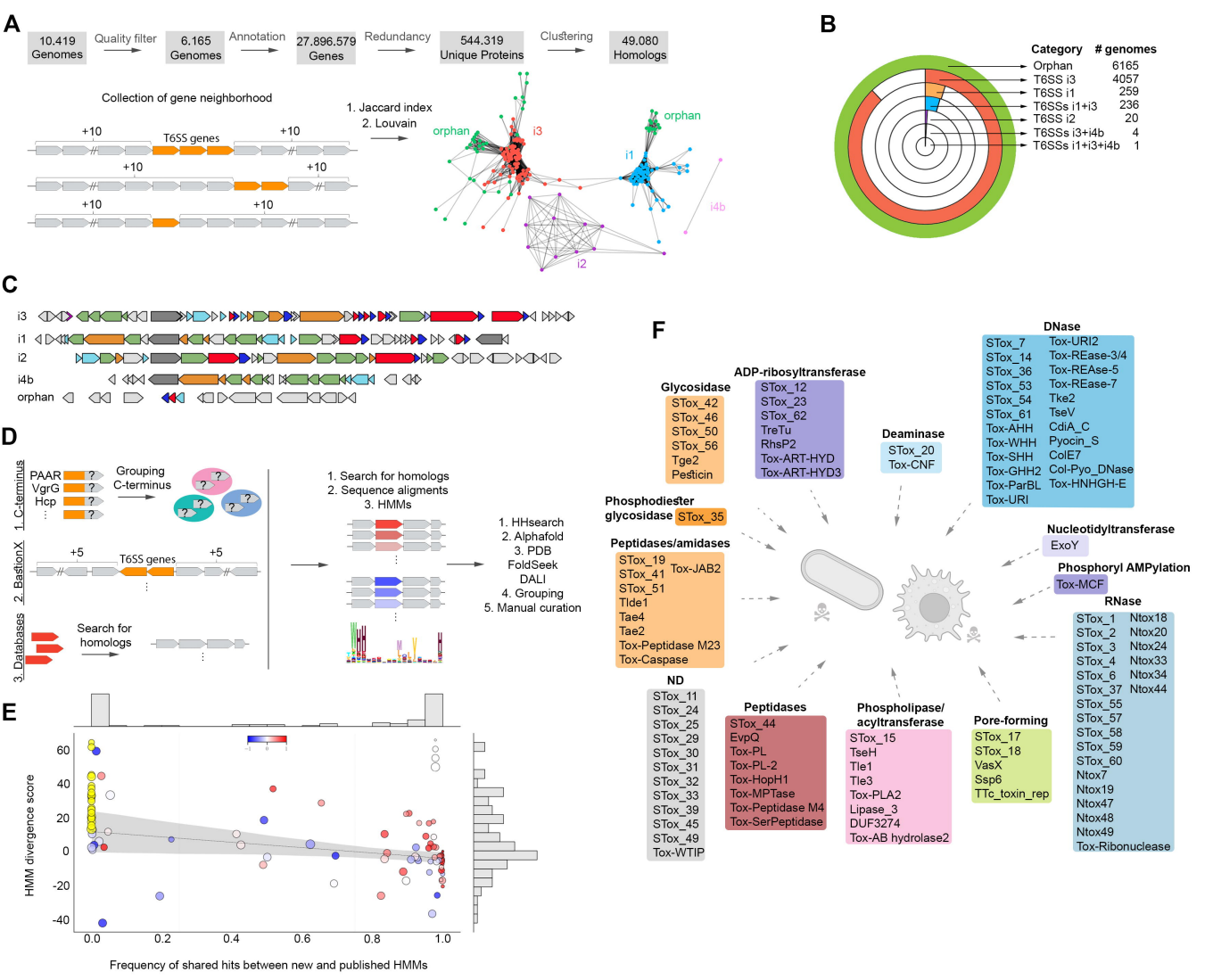
A
10.419 Genomes
Quality filter
6.165 Genomes
Annotation
27,896,579 Genes
Redundancy
544.319 Unique Proteins
Clustering
49.080 Homologs
Collection of gene neighborhood
+10
T6SS genes
1. Jaccard index
2. Louvain
orphan
i3
i1
i2
i4b
B
Category # genomes
Orphan 6165
T6SS i3 4057
T6SS i1 259
T6SSs i1+i3 236
T6SS i2 20
T6SSs i3+i4b 4
T6SSs i1+i3+i4b 1
C
i3
i1
i2
i4b
orphan
D
PAAR
VgrG
Hcp
Grouping C-terminus
1. C-terminus
2. BastionX
3. Databases
+5
T6SS genes
Search for homologs
1. Search for homologs
2. Sequence aligments
3. HMMs
1. HHsearch
2. Alphafold
3. PDB
FoldSeek
DALI
4. Grouping
5. Manual curation
E
HMM divergence score
Frequency of shared hits between new and published HMMs
F
Glycosidase
STox_42
STox_46
STox_50
STox_56
Tge2
Pesticin
ADP-ribosyltransferase
STox_12
STox_23
STox_62
TreTu
RhsP2
Tox-ART-HYD
Tox-ART-HYD3
Deaminase
STox_20
Tox-CNF
DNase
STox_7
STox_14
STox_36
STox_53
STox_54
STox_61
Tox-AHH
Tox-WHH
Tox-SHH
Tox-GHH2
Tox-ParBL
Tox-URI
Tox-URI2
Tox-REase-3/4
Tox-REAse-5
Tox-REase-7
Tke2
TseV
CdiA_C
Pyocin_S
ColE7
Col-Pyo_DNase
Tox-HNHGH-E
Phosphodiester glycosidase
STox_35
Peptidases/amidases
STox_19
STox_41
STox_51
Tox-JAB2
Tlde1
Tae4
Tae2
Tox-Peptidase M23
Tox-Caspase
Nucleotidyltransferase
ExoY
Phosphoryl AMPylation
Tox-MCF
RNase
STox_1
STox_2
STox_3
STox_4
STox_6
STox_37
STox_55
STox_57
STox_58
STox_59
STox_60
Ntox7
Ntox19
Ntox47
Ntox48
Ntox49
Tox-Ribonuclease
Ntox18
Ntox20
Ntox24
Ntox33
Ntox34
Ntox44
ND
STox_11
STox_24
STox_25
STox_29
STox_30
STox_31
STox_32
STox_33
STox_39
STox_45
STox_49
Tox-WTIP
Peptidases
STox_44
EvpQ
Tox-PL
Tox-PL-2
Tox-HopH1
Tox-MPTase
Tox-Peptidase M4
Tox-SerPeptidase
Phospholipase/ acyltransferase
STox_15
TseH
Tle1
Tle3
Tox-PLA2
Lipase_3
DUF3274
Tox-AB hydrolase2
Pore-forming
STox_17
STox_18
VasX
Ssp6
TTc_toxin_rep

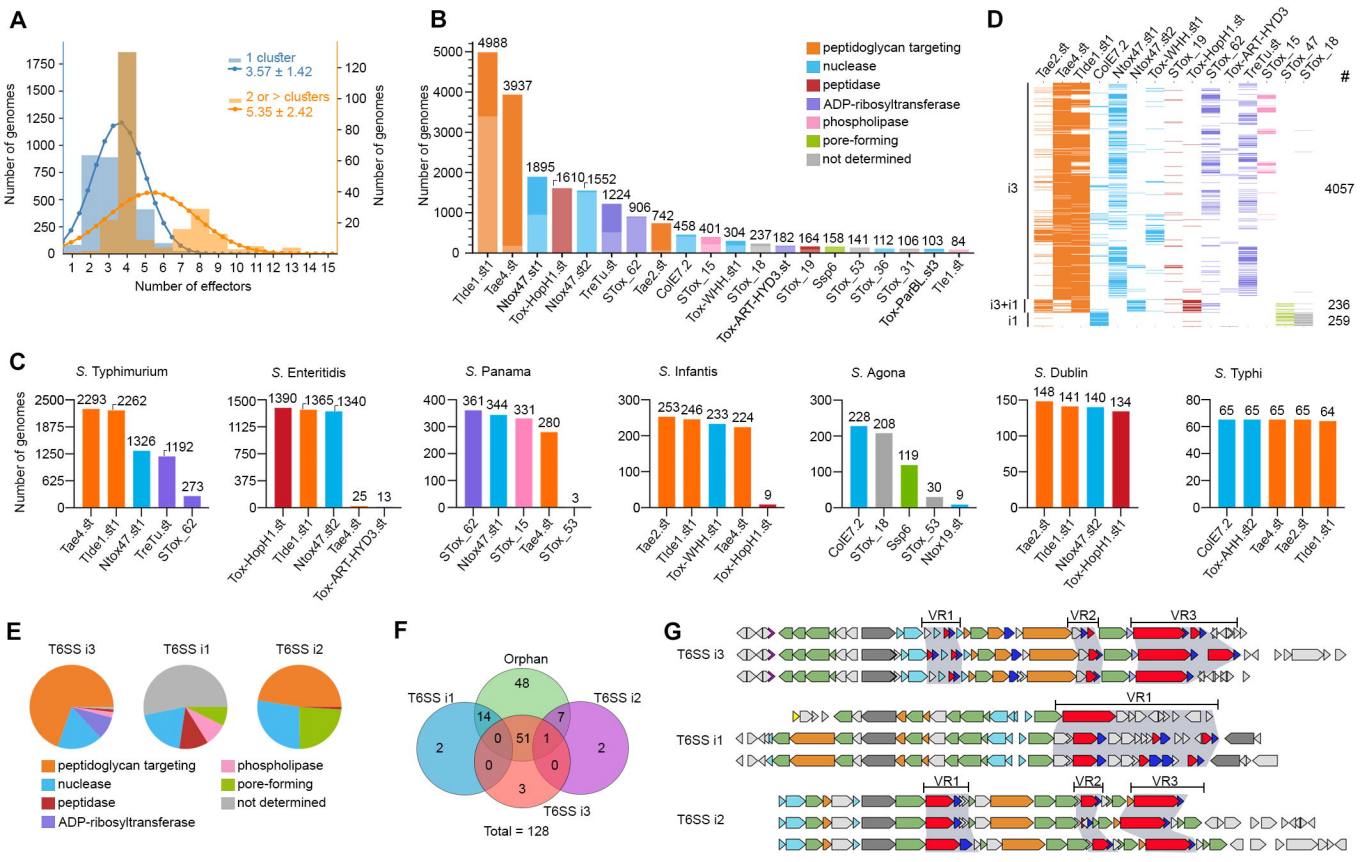
A
1 cluster
3.57 ± 1.42
2 or > clusters
5.35 ± 2.42
Number of genomes
Number of effectors
B
peptidoglycan targeting
nuclease
peptidase
ADP-ribosyltransferase
phospholipase
pore-forming
not determined
4988
3937
1895
1610
1552
1224
906
742
458
401
304
237
182
164
158
141
112
106
103
84
Tlde1.st1
Tae4.st
Ntox47.st1
Tox-HopH1.st
Ntox47.st2
TreTu.st
STox_62
Tae2.st
ColE7.2
STox_15
Tox-WHH.st1
STox_18
Tox-ART-HYD3.st
STox_19
Ssp6
STox_53
STox_36
STox_31
Tox-PafBL.st3
Tle1.st
D
Tae2.st
Tae4.st
Tlde1.st1
ColE7.2
Ntox47.st1
Ntox47.st2
Tox-WHH.st1
STox_19
Tox-HopH1.st
STox_62
Tox-ART-HYD3
TreTu.st
STox_15
STox_47
STox_18
#
i3
4057
i3+i1
236
i1
259
C
S. Typhimurium
2293
2262
1326
1192
273
Tae4.st
Tlde1.st1
Ntox47.st1
TreTu.st
STox_62
S. Enteritidis
1390
1365
1340
25
13
Tox-HopH1.st
Tlde1.st1
Ntox47.st2
Tae4.st
Tox-ART-HYD3.st
S. Panama
361
344
331
280
3
STox_62
Ntox47.st1
STox_15
Tae4.st
STox_53
S. Infantis
253
246
233
224
9
Tae2.st
Tlde1.st1
Tox-WHH.st1
Tae4.st
Tox-HopH1.st
S. Agona
228
208
119
30
9
ColE7.2
STox_18
Ssp6
STox_53
Ntox19.st
S. Dublin
148
141
140
134
Tae2.st
Tlde1.st1
Ntox47.st2
Tox-HopH1.st1
S. Typhi
65
65
65
65
64
ColE7.2
Tox-AHH.st2
Tae4.st
Tae2.st
Tlde1.st1
Number of genomes
E
T6SS i3
T6SS i1
T6SS i2
peptidoglycan targeting
nuclease
peptidase
ADP-ribosyltransferase
phospholipase
pore-forming
not determined
F
Orphan
T6SS i1
T6SS i2
T6SS i3
48
14
7
2
0
51
1
2
0
3
0
Total = 128
G
VR1
VR2
VR3
T6SS i3
T6SS i1
T6SS i2

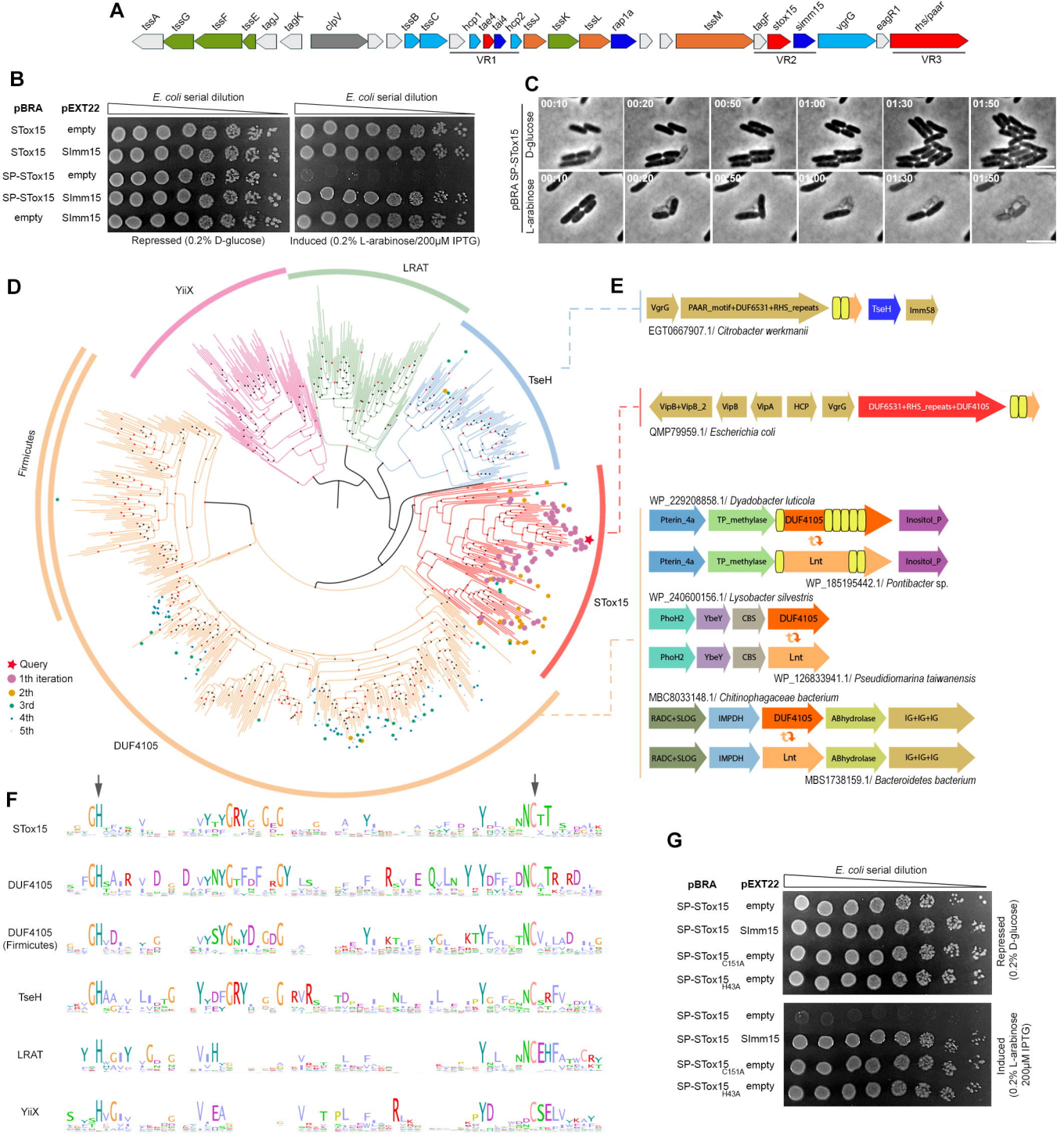
A
tssA
tssG
tssF
tssE
tagJ
tagK
clpV
tssB
tssC
hcp1
tae4
taf4
hcp2
tssJ
tssK
tssL
rap1a
tssM
tagF
stox15
slmm15
vgrG
eagR1
rhs/paar
VR1
VR2
VR3
B
pBRA
pEXT22
E. coli serial dilution
E. coli serial dilution
STox15
empty
STox15
SImm15
SP-STox15
empty
SP-STox15
SImm15
empty
SImm15
Repressed (0.2% D-glucose)
Induced (0.2% L-arabinose/200μM IPTG)
C
pBRA SP-STox15
D-glucose
L-arabinose
00:10
00:20
00:50
01:00
01:30
01:50
D
LRAT
YiiX
TseH
STox15
DUF4105
Firmicutes
Query
1th iteration
2th
3rd
4th
5th
E
VgrG
PAAR_motif+DUF6531+RHS_repeats
TseH
Imm58
EGT0667907.1/ Citrobacter werkmanii
VipB+VipB_2
VipB
VipA
HCP
VgrG
DUF6531+RHS_repeats+DUF4105
QMP79959.1/ Escherichia coli
WP_229208858.1/ Dyadobacter luticola
Pterin_4a
TP_methylase
DUF4105
Inositol_P
Pterin_4a
TP_methylase
Lnt
Inositol_P
WP_185195442.1/ Pontibacter sp.
WP_240600156.1/ Lysobacter silvestris
PhoH2
YbeY
CBS
DUF4105
PhoH2
YbeY
CBS
Lnt
WP_126833941.1/ Pseudidiomarina taiwanensis
MBC8033148.1/ Chitinophagaceae bacterium
RADC+SLOG
IMPDH
DUF4105
ABhydrolase
IG+IG+IG
RADC+SLOG
IMPDH
Lnt
ABhydrolase
IG+IG+IG
MBS1738159.1/ Bacteroidetes bacterium
F
STox15
DUF4105
DUF4105 (Firmicutes)
TseH
LRAT
YiiX
G
pBRA
pEXT22
E. coli serial dilution
SP-STox15
empty
SP-STox15
SImm15
SP-STox15 C151A
empty
SP-STox15 H43A
empty
Repressed (0.2% D-glucose)
SP-STox15
empty
SP-STox15
SImm15
SP-STox15 C151A
empty
SP-STox15 H43A
empty
Induced (0.2% L-arabinose 200μM IPTG)

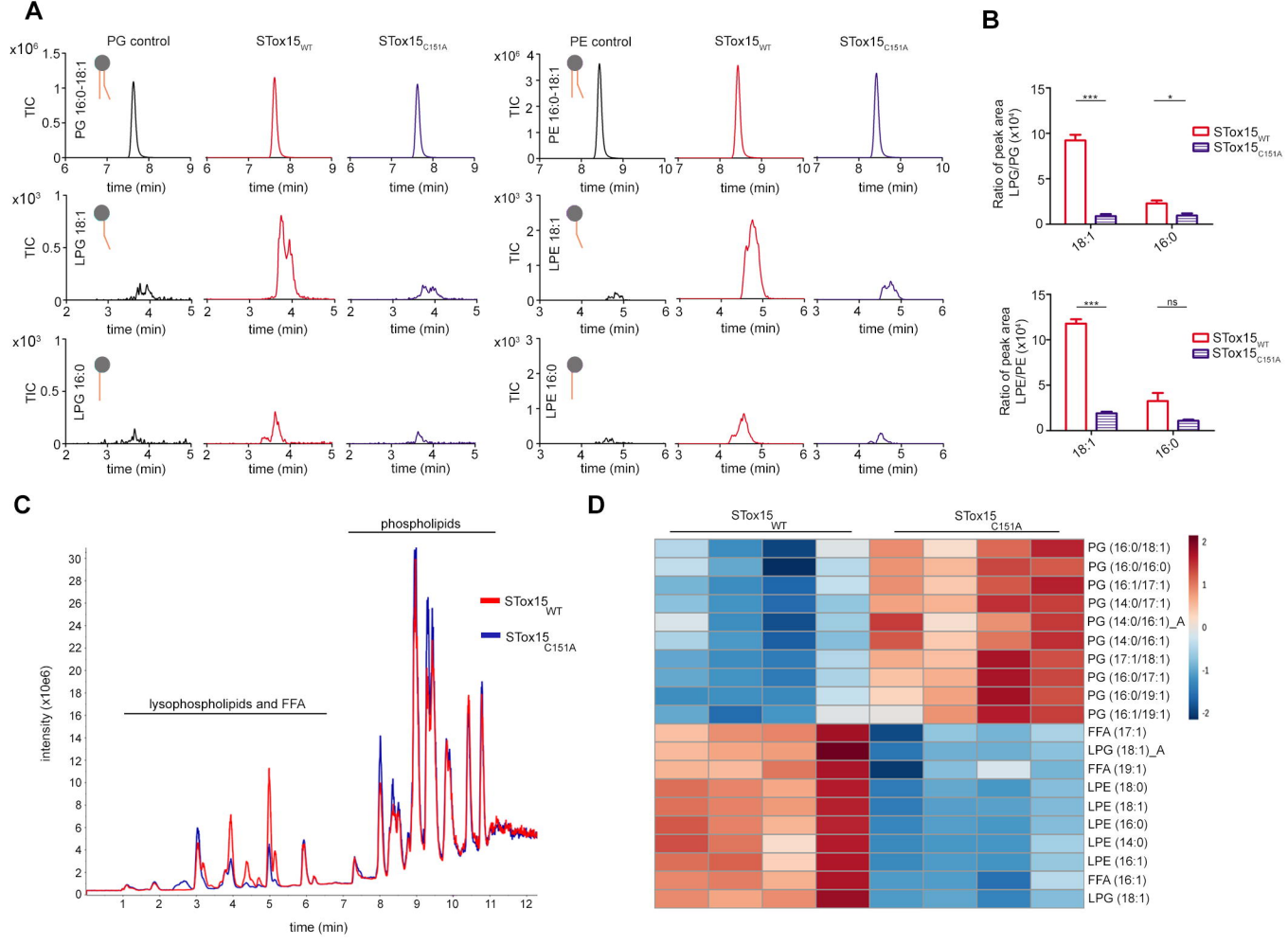
A
PG control
STox15WT
STox15C151A
PE control
PG 16:0-18:1
PE 16:0-18:1
LPG 18:1
LPE 18:1
LPG 16:0
LPE 16:0
TIC
time (min)
B
Ratio of peak area LPG/PG (x10⁴)
Ratio of peak area LPE/PE (x10⁴)
18:1
16:0
***
*
ns
C
phospholipids
lysophospholipids and FFA
intensity (x10e6)
time (min)
D
PG (16:0/18:1)
PG (16:0/16:0)
PG (16:1/17:1)
PG (14:0/17:1)
PG (14:0/16:1)_A
PG (14:0/16:1)
PG (17:1/18:1)
PG (16:0/17:1)
PG (16:0/19:1)
PG (16:1/19:1)
FFA (17:1)
LPG (18:1)_A
FFA (19:1)
LPE (18:0)
LPE (18:1)
LPE (16:0)
LPE (14:0)
LPE (16:1)
FFA (16:1)
LPG (18:1)